Subseasonal Prediction of Extreme Precipitation over Asia: Boreal Summer Intraseasonal Oscillation Perspective

Sun-Seon Lee and Ja-Yeon Moon

Department of Atmospheric Sciences, International Pacific Research Center, and Atmosphere–Ocean Research Center, University of Hawai'i at Mānoa, Honolulu, Hawaii

Bin Wang

Department of Atmospheric Sciences, and International Pacific Research Center, and Atmosphere–Ocean Research Center, University of Hawai'i at Mānoa, Honolulu, Hawaii, and Earth System Modeling Center, Nanjing University of Information Science and Technology, Nanjing, China

Hae-Jeong Kim

Asia–Pacific Economic Cooperation (APEC) Climate Center (APCC), Busan, South Korea

(Manuscript received 9 March 2016, in final form 29 September 2016)

ABSTRACT

The boreal summer intraseasonal oscillation (BSISO) is one of the most prominent modes in the tropical climate system. For better subseasonal prediction of extreme precipitation the relationship between BSISO activity and extreme precipitation events (days with daily precipitation exceeding the local 90th percentile) over Asia is investigated, especially the dependence of extreme precipitation occurrence on BSISO precipitation anomaly pattern (phase) and intensity (amplitude) in each month. At a given area and month, the probability of extreme precipitation changes from less than 10% to over 40%–50% according to BSISO phases, and it tends to be high when BSISO amplitude is large. The extreme precipitation probability estimated by BSISO activity is generally higher over ocean than over land. Over some land regions, however, occurrence of extreme precipitation is notably modulated by BSISO activity. In May, the extreme precipitation probability over southeastern China can reach about 30%–40% when BSISO precipitation anomaly arrives over the region. Similarly, in September the extreme precipitation probability over western China can reach 40%–50% when BSISO precipitation anomaly arrives there. The BSISO activity provides useful information in narrowing down the area and timing of high probability of extreme precipitation occurrence. Using real-time BSISO monitoring and forecast data provided by the Asia–Pacific Economic Cooperation (APEC) Climate Center, it is shown that 1) the best model (ECMWF) can predict the leading BSISO modes about 20 days ahead with bivariate correlation skills higher than 0.5 except in May, and 2) the empirical probability distributions of extreme precipitation that are based on BSISO activity can be captured by the BSISO forecasts for lead times longer than 2 weeks.

1. Introduction

Prediction of extreme weather events such as heavy precipitation, drought, heat waves, and tropical cyclones is an important subject since extreme events can cause severe property damage and loss of human life (e.g., Vitart et al. 2012). In particular, occurrences of extreme precipitation on subseasonal time scale have enormous impacts on our communities. For the period 1998–2008, around 247 000 people worldwide were killed due to flood events (Adhikari et al. 2010). Asia is one of the most vulnerable regions to flood. The economic loss caused by floods in Bangladesh in a normal year is about $175 million (Jonkman 2005; Mirza 2011). In addition, positive trends in frequency and intensity of extreme precipitation events have been found in many parts of Asia (e.g., Sen Roy and Balling 2004; Zhai et al. 2005; Goswami et al. 2006; Wang et al. 2006; Endo et al. 2009; Krishnamurthy et al. 2009; Yao et al. 2010; Mirza 2011).

School of Ocean and Earth Science and Technology Publication Number 9889, International Pacific Research Center Publication Number 1232, and Earth System Modeling Center Publication Number 143.

Corresponding author e-mail: Prof. Bin Wang, wangbin@hawaii.edu

DOI: 10.1175/JCLI-D-16-0206.1

Sen Roy and Balling (2004) analyzed daily precipitation records throughout India over the period 1910–2000 and showed increase in extreme precipitation events, including total precipitation, the largest 1-, 5-, and 30-day totals, and the number of daily events above the 90th, 95th, and 97.5th percentiles of all precipitation. Increases in intensity and frequency of extreme rainfall events result in considerable social and economic damages (e.g., Kundzewicz et al. 2014; Dewan 2015). Therefore, societal and economic demands for understanding, monitoring, and predicting extreme weather events have been increasing rapidly.

Since extreme precipitation events occur on multiple spatial and temporal scales, it is difficult to predict their occurrences. During boreal winter, the Madden–Julian oscillation (MJO) is the prominent mode of tropical intraseasonal variability (e.g., Waliser 2006; Goswami 2011). Therefore, MJO activity has been considered a major source of predictability for extreme weather events. Many previous studies show that the MJO modulates extreme weather events such as extreme rainfall, snowfall, cold surges, and tropical storms on global and regional scales (e.g., Jones et al. 2004; Jones and Carvalho 2012; Moon et al. 2012; Zhou et al. 2012; Zhang 2013; Xavier et al. 2014; Wang and Moon 2017).

In addition to the MJO, the boreal summer intraseasonal oscillation (BSISO) is one of the dominant factors modulating occurrences of extreme events over the Asian-Pacific monsoon region. The BSISO is closely related to various spatiotemporal drivers of weather variability including tropical cyclones, monsoon active–break cycles, and extratropical circulation anomalies in the Northern Hemisphere (e.g., Liebmann et al. 1994; Wang and Xu 1997; Wu and Wang 2000; Maloney and Hartmann 2001; Goswami et al. 2003; Goswami 2011; Moon et al. 2013). Zhu et al. (2003) showed that a series of severe floods in eastern China in 1998 was related to the activity of the 30–60-day BSISO over the western North Pacific (WNP). It is noted that the collective influences of a northward propagation of the 30–60-day BSISO from the equatorial Indian Ocean and a westward propagation of the 10–20-day disturbance from the South China Sea are among the prominent atmospheric processes to lead extreme active and break rainfall phases in northern India (Ding and Wang 2009).

To better monitor and predict BSISO activity over the Asian summer monsoon region, Lee et al. (2013) proposed two BSISO indices based on multivariate empirical orthogonal function (MV-EOF) analysis (Wang 1992) using daily anomalies of OLR and 850-hPa zonal wind over the Asian monsoon sector (10°S–40°N, 40°–160°E). BSISO1 (EOF1 and EOF2 modes) represents the canonical northward propagating BSISO during the entire warm season (from May to October) with quasi-oscillating periods of 30–60 days. BSISO2 (EOF3 and EOF4 modes) mainly captures the northward or northwestward propagation component with a 10–30-day spectral peak, and shows maximum variance from late May to early July. Recently, Hsu et al. (2016) examined the influences of BSISO modes on the spatial distributions of extreme rainfall in southeastern China. The probability of extreme rainfall events exceeding the 75th and 90th percentile increases mostly over the Yangtze River valley during phases 2–4 of BSISO1.

Given the increasing demands and importance of forecasting extreme precipitation events, our study aims to establish the relationship between BSISO activity and extreme precipitation events over Asia in order to detect and predict extreme precipitation occurrence using BSISO information in subseasonal time scale. From a prediction perspective, it would be useful to provide the probability of extreme precipitation events as a function of BSISO activity. In the present study, we estimate the probabilities of extreme precipitation events using observed and predicted BSISO modes, respectively. Using real-time BSISO forecast data provided by the Asia–Pacific Economic Cooperation (APEC) Climate Center (APCC), we assess prediction skill of leading BSISO modes and the capability of BSISO forecasts for capturing empirical relationship between BSISO activity and extreme precipitation events.

This paper is organized as follows. Section 2 describes the data and analysis methods. In section 3, we show the climatological spatiotemporal features of extreme precipitation events and BSISO evolution with the seasonal march. Section 4 presents the relationship between BSISO activity and extreme precipitation events, and BSISO-based probability of extreme events. The prediction skill of leading BSISO modes and probability of extreme events estimated by BSISO forecasts are given in section 5. The last section is a summary and discussion.

2. Data and analysis methods

a. Data

1) PRECIPITATION

To identify the extreme events in terms of precipitation, we use daily Global Precipitation Climatology Project (GPCP) data (Huffman and Bolvin 2013)

TABLE 1. Model names and description of BSISO forecasts of APCC.

Model	Institution	Initializations	Ensemble size	Analysis period
Predictive Ocean Atmosphere Model for Australia, version 2.4 (POAMA-2.4) multiweek model (BOM)	Australian Bureau of Meteorology	Twice per week	33	From May to October 2013–15
Climate Forecast System (CFS)	National Centers for Environmental Prediction	Every day	4	From May to October 2013–15
ECMWF Ensemble Prediction System (ECM)	European Centre for Medium-Range Weather Forecasts	Twice per week	51	From May to October 2013–15

for the period 1997–2015 (19 yr), which have 1° × 1° resolution. The target region is selected as 0°–40°N, 70°–140°E and the boreal summer period from May to October is considered.

2) BSISO INDICES

To represent BSISO activity over the Asian summer monsoon region, we use two real-time multivariate indices (i.e., BSISO1 and BSISO2) proposed by Lee et al. (2013). BSISO1 (BSISO2) is defined by the first and second (third and fourth) principal components (PCs) of the MV-EOF analysis. To show the evolution and propagation of BSISO1 (BSISO2), eight phases are defined based on sign and amplitude of PC1 and PC2 (PC3 and PC4) (Lee et al. 2013). In this study, the definition of BSISO's eight phases follows Lee et al. (2013).

General features of BSISO evolution are as follows. Convection anomaly associated with BSISO1 appears over the equatorial Indian Ocean in phase 1, and then propagates northeastward. It reaches the Indian subcontinent in phase 3 and the Bay of Bengal in phases 4 and 5. During these phases, convection anomaly is characterized by the northwest–southeast-tilted rainband. Then, convection anomaly over the Maritime Continent and equatorial western Pacific propagates northward and reaches the South China Sea in phase 7 and the WNP in phase 8. For BSISO2, the convection anomaly is located in the equatorial Indian Ocean and Philippine Sea in phase 1. Then, it propagates northwestward over the Indian Ocean and WNP–East Asian (EA) regions. In phases 4 and 5 convection anomaly shows a southwest–northeast-tilted horizontal structure from the Bay of Bengal to the WNP–EA region. For further details of the BSISO indices, the readers are referred to Lee et al. (2013).

In APCC, real-time BSISO forecast activity is initiated in 2013 for improving the ability to understand and forecast BSISO (http://www.apcc21.org/ser/casts.do?lang=en). Real-time BSISO forecasts produced by three operational numerical models from APCC are used as a counterpart to observed BSISO indices. In the present study, these models are named simply BOM (from the Australian Bureau of Meteorology; Hudson et al. 2013), CFS (from NCEP; Saha et al. 2014), and ECM (from ECMWF; Buizza et al. 2005) in the present study. The models provided by APCC together with a description of BSISO forecast setup are presented in Table 1.

b. *Analysis methods*

1) EXTREME PRECIPITATION: DEFINITION AND ESTIMATION OF PROBABILITY USING BSISO MODES

As the flooding events are observed to have seasonal variation (Adhikari et al. 2010), we calculate the extreme precipitation threshold in each month. For each month, we select precipitation events with greater than 0.3 mm day^{-1} of daily precipitation. Dry regions where the climatological monthly mean precipitation rate is less than 2 mm day^{-1} are excluded in our analysis. With these considerations, the daily precipitation at individual grid point for each month fits in an approximate gamma distribution. The 90th percentile is used as threshold value to define the extreme precipitation events. The spatial distribution of 90th percentile precipitation in each month is shown in Fig. 1b and its pattern is very similar to 95th percentile precipitation (not shown).

The empirical probability of extreme precipitation events is estimated using observed BSISO indices. Using 19 years of precipitation and BSISO index data, we estimate the BSISO phase-dependent (P-dependent) probability of extreme precipitation:

$$\text{P-dependent Pr\_O}(\%) = P(\text{Ext} \,|\, \text{BSISO\_}XZ), \quad (1)$$

where Pr_O denotes estimation of extreme precipitation probability using observed BSISO indices, P(BSISO_XZ) indicates the probability of BSISO phase X occurrence in a certain month Z, and P(Ext | BSISO_XZ) represents

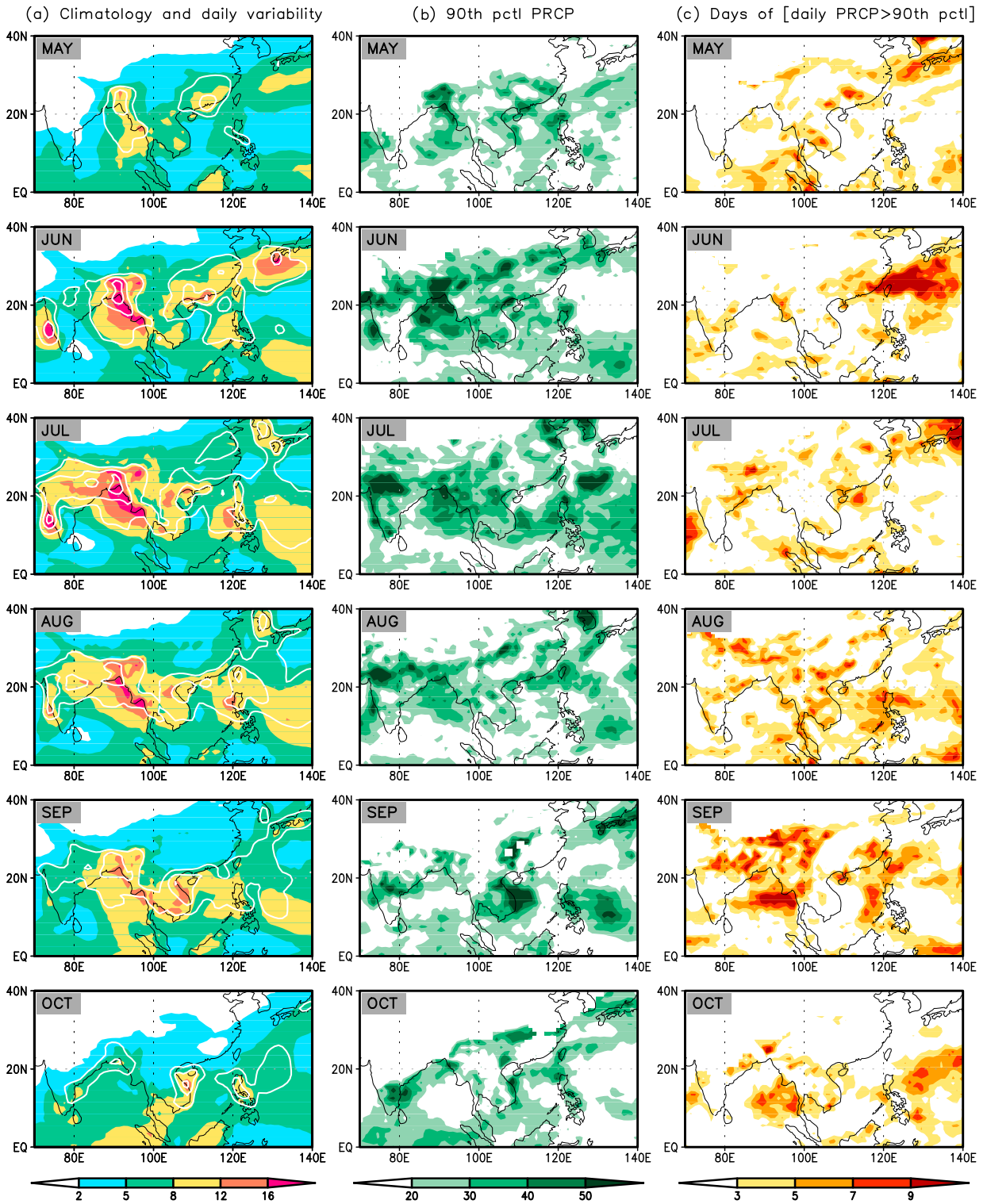

FIG. 1. (a) Climatology (shading) and daily variability (white contour, ≥12 mm day^{-1}, interval: 4 mm day^{-1}) of precipitation in each month (1997–2015). (b) The 90th percentile precipitation (mm day^{-1}) as a threshold of extreme precipitation. (c) Mean occurrence days (occurrence days averaged over 19 yr) of extreme precipitation events.

the conditional probability of extreme precipitation occurrence when BSISO phase is X in a month Z.

Further, to consider the effects of BSISO amplitude on extreme precipitation occurrence, the BSISO phase–amplitude (PA)-dependent probability is calculated. For this calculation, BSISO index data are classified into four groups according to large and small BSISO amplitudes, namely $(PC1^2 + PC2^2)^{1/2} \geq 1.0$, $(PC1^2 + PC2^2)^{1/2} < 1.0$, $(PC3^2 + PC4^2)^{1/2} \geq 1.0$, and $(PC3^2 + PC4^2)^{1/2} < 1.0$. The PA-dependent probability estimated by observed BSISO phase and amplitude at a given month can be obtained by:

$$\text{PA-dependent Pr\_O}(\%) = P(\text{Ext} \,|\, \text{BSISO\_}XYZ), \quad (2)$$

where P(BSISO_XYZ) is the probability that BSISO phase X, which meets the amplitude criteria Y, occurs in a certain month Z.

Similar to the estimation of extreme precipitation probability using observed BSISO indices (i.e., Pr_O), we examine the corresponding probability using predicted BSISO indices (Pr_F). For this analysis, we classify four forecast groups according to the forecast lead time, on which forecast capability depends: "weather forecast" with 0–3 forecast lead days, "pentad 1 forecast" with 4–8 forecast lead days, "pentad 2 forecast" with 9–13 forecast lead days, and "pentad 3 forecast" with 14–18 forecast lead days. Using BSISO forecast data and observed precipitation, the P-dependent and PA-dependent probabilities of extreme precipitation events can be calculated by:

$$\text{P-dependent Pr\_F}(\%) = P(\text{Ext} \,|\, \text{BSISO}_{F}\text{\_}XZ) \quad \text{and} \quad (3)$$

$$\text{PA-dependent Pr\_F}(\%) = P(\text{Ext} \,|\, \text{BSISO}_{F}\text{\_}XYZ), \quad (4)$$

where $P(\text{BSISO}_{F}\text{\_}XZ)$ indicates the probability that predicted BSISO phase is X in a certain month Z, and $P(\text{Ext} \,|\, \text{BSISO}_{F}\text{\_}XZ)$ represents the probability that extreme precipitation occurs in observation when the predicted BSISO phase is X in a month Z. Because of the limited data length of BSISO forecasts, the probability is calculated using the data for summer from 2013 to 2015. Although the forecast data for three seasons are not long enough to evaluate prediction capability, the present study attempts to show the potential for monitoring and forecasting extreme precipitation events using real-time BSISO forecast data.

2) FORECAST SKILL OF BSISO MODES

The forecast skill of BSISO indices is assessed in terms of bivariate correlation [Eq. (5)], which measures the linear relationship between PC pairs (Lin et al. 2008; Gottschalck et al. 2010). We use the ensemble mean for this analysis:

$$\text{Corr}(\tau) = \frac{\sum_{i=1}^{N} [a_1(t) b_{1i}(t,\tau) + a_{2i}(t) b_{2i}(t,\tau)]}{\sqrt{\sum_{i=1}^{N} [a_1^2(t) + a_2^2(t)]} \sqrt{\sum_{i=1}^{N} [b_{1i}^2(t,\tau) + b_{2i}^2(t,\tau)]}}, \quad (5)$$

where $a_1(t)$ and $a_2(t)$ are the observed BSISO PC1 and PC2 (or BSISO PC3 and PC4) at day t, and $b_{1i}(t, \tau)$ and $b_{2i}(t, \tau)$ are their respective forecasts at day t for a lead time of τ days. Here, N is the number of forecasts.

3. Seasonal march of mean precipitation, extreme events, and BSISO evolution

Understanding the climatological features and daily variability of precipitation over Asia is necessary before examining the features of extreme precipitation events. Figure 1a presents the spatial distribution of climatology and daily standard deviation of precipitation in each month from May to October. It is noted that both climatology and daily variability of precipitation change with the seasonal march. Major rainbands in South and Southeast Asia are enhanced and propagate northwestward from May to August and weaken from September to October. Daily variability is strong over land, land–ocean boundaries, and the WNP, particularly the 10°–30°N band. However, over the equatorial eastern Indian Ocean and WNP monsoon trough (intertropical convergence zone), daily variability is weak, which indicates high mean precipitation is not necessarily linked to large daily variability over those regions. The distribution of daily variability is likely related to the distributions of synoptic-scale and intraseasonal oscillation (ISO) variability. The synoptic-scale variability is much larger over the land and land–ocean boundary regions, but ISO variability is great over oceans (not shown).

Figures 1b and 1c exhibit the 90th percentile precipitation as a threshold of extreme precipitation events and mean occurrence days of extreme events, respectively. In general, the 90th percentile precipitation tends to be large over the regions of major rainbands and strong daily variability (Fig. 1b). Similar to the climatology and daily variability, occurrences of extreme precipitation events show distinct intraseasonal changes (Fig. 1c). Climatologically, extreme precipitation events are observed most frequently over the East China Sea in June and northern Indian Ocean in September (more than 10 days in a month).

Characteristics of BSISO activity, such as the life cycle and location of maximum amplitude, change with the

seasonal march (e.g., Kemball-Cook and Wang 2001; Liu and Wang 2014; Lee and Wang 2016). Therefore, before exploring the relationship between BSISO activity and extreme precipitation events, we examine the subseasonal features of BSISO evolution. Figure 2 shows the number of occurrence days for each phase of BSISO1 and BSISO2. The composite precipitation anomaly related to the most frequently occurring BSISO phase is also presented. It is worth noting that several phases show a distinct time preference for their occurrence (Lee and Wang 2016). In May, phase 7 of BSISO1, which shows strong positive precipitation anomaly from the South China Sea to WNP (Fig. 2g), is observed 122 days out of total 589 days (31 days × 19 yr), but phase 4 is found in only 42 days. In August, phase 2 of BSISO1, which shows a strong dry anomaly over the Bay of Bengal and WNP (Fig. 2h), occurs on 122 days whereas phase 1 occurs on 41 days. In September and October, phases 5 and 1 of BSISO1 are the most frequently occurring phases, respectively, and their spatial patterns of precipitation anomaly are nearly opposite (Figs. 2i,j). The phase preference of BSISO1 is relatively weak in June and July compared to other months, but BSISO2 shows a strong phase preference in these months. In June, phase 6 of BSISO2, which has a positive precipitation anomaly in southeastern China and the Bay of Bengal (Fig. 2k), shows the highest frequency with 123 days. Phase 8 of BSISO2 (Fig. 2l) occurs for 110 days in July. Reasons for the phase preference of BSISO activity are of interest and will be further discussed in the last section.

Furthermore, BSISO evolution from phase 1 to phase 8 reflects the seasonal shift. In general, BSISO precipitation anomalies evolve northeastward over the Indian Ocean sector and northward over the western Pacific from phase 1 to phase 8, but the location of maximum amplitude of ISO activity changes with the seasonal march. In May a strong positive precipitation anomaly prevails over the equatorial Indian Ocean from phase 2 to phase 4 (Fig. 3a), whereas in August the most dominant precipitation anomaly is observed over the WNP from phase 6 to phase 8 (not shown).

4. Empirical relationship between BSISO and extreme precipitation events

Establishing useful linkages between BSISO activity and extreme precipitation events is important for subseasonal prediction of extreme events. To find out whether BSISO activity can be indicative of extreme precipitation occurrence, the probability of extreme precipitation events is estimated as a function of BSISO phase and amplitude. The present study will mainly discuss the results related to BSISO1 mode.

Figure 3 presents the precipitation anomaly, P-dependent probability, and PA-dependent probability (case of large BSISO amplitude) according to BSISO1 phases in May. Note that the probability of extreme precipitation over a certain area substantially changes with BSISO1 phases. For example, the P-dependent probability is about 30%–40% in the equatorial Indian Ocean when BSISO1 phases are 2 and 3. However, it is less than 10% over the corresponding region in BSISO1 phase 7. In addition, the probability tends to be higher if we consider both BSISO phase and large amplitude (PA-dependent probability).

Several phases, such as phases 2–4, exhibit high spatial similarity between BSISO precipitation anomaly and extreme precipitation probability pattern (i.e., regions with a strong precipitation anomaly correspond to regions of high probability). However, some phases such as phase 8 show low spatial coherence between the two fields. To select key phases that show high spatial similarity between BSISO precipitation anomaly and extreme precipitation probability pattern, we examine pattern correlation coefficients (PCCs) between BSISO precipitation anomaly field and P-dependent probability distribution over 0°–40°N, 70°–140°E. For the PCC calculation, we consider the grid points where precipitation anomalies are positive only. BSISO1 phases are ordered by the PCC in each month and the top three BSISO1 phases are presented in Figs. 4 and 5. In all selected phases, the spatial patterns of P-dependent probabilities are very similar to precipitation anomaly fields. This indicates that, during these phases, regions with strong precipitation anomalies have higher chances of reaching the extreme stage.

In May, strong precipitation anomaly during phases 2–4 (Fig. 4a) may mainly contribute to the distribution of extreme event occurrence shown in Fig. 2c. In June, precipitation anomalies during BSISO1 phase 8 and phase 1 are very strong over the East China Sea (Fig. 4b) and it is consistent with spatial pattern of extreme event days in the corresponding month (Fig. 2c). In most cases, high probabilities are observed over ocean. However, it is interesting to note that probability over some land regions is largely controlled by BSISO activity. The extreme precipitation probability over southeastern China is about 30%–40% in May when the BSISO precipitation anomaly arrives over the corresponding region (phase 4). Similarly, the probability of extreme precipitation over western China reaches 40%–50% in September when the BSISO precipitation anomaly arrives over the region (phase 1). The probability over Indochina is 20%–30% during phase 6 in October.

Similar to BSISO1, BSISO2 phases are ranked by PCC between precipitation anomaly and probability

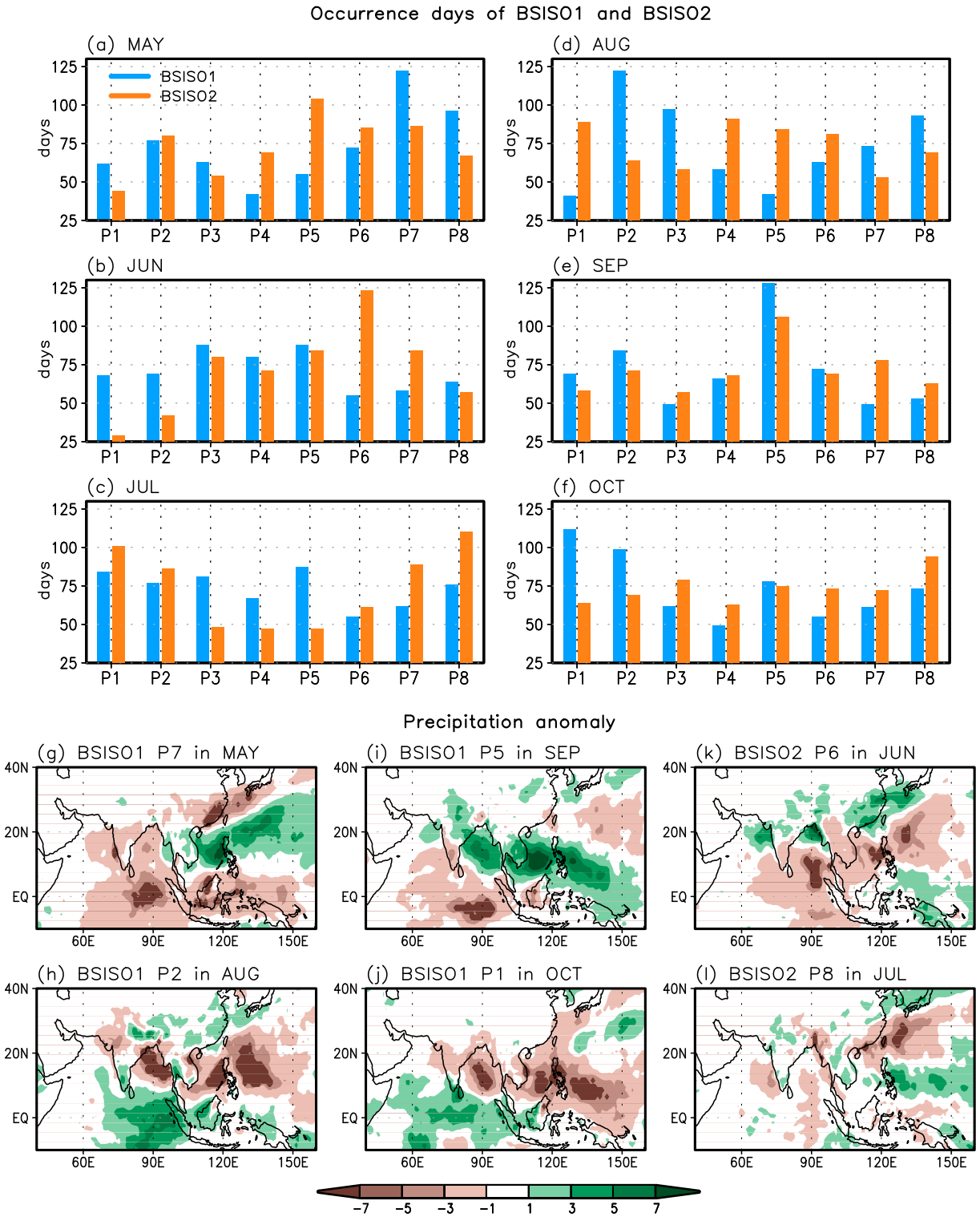

FIG. 2. (a)–(f) Total occurrence days of each BSISO phase in a given month (1997–2015). (g)–(l) Precipitation anomaly (mm day^{-1}) at the most frequently occurring BSISO phase.

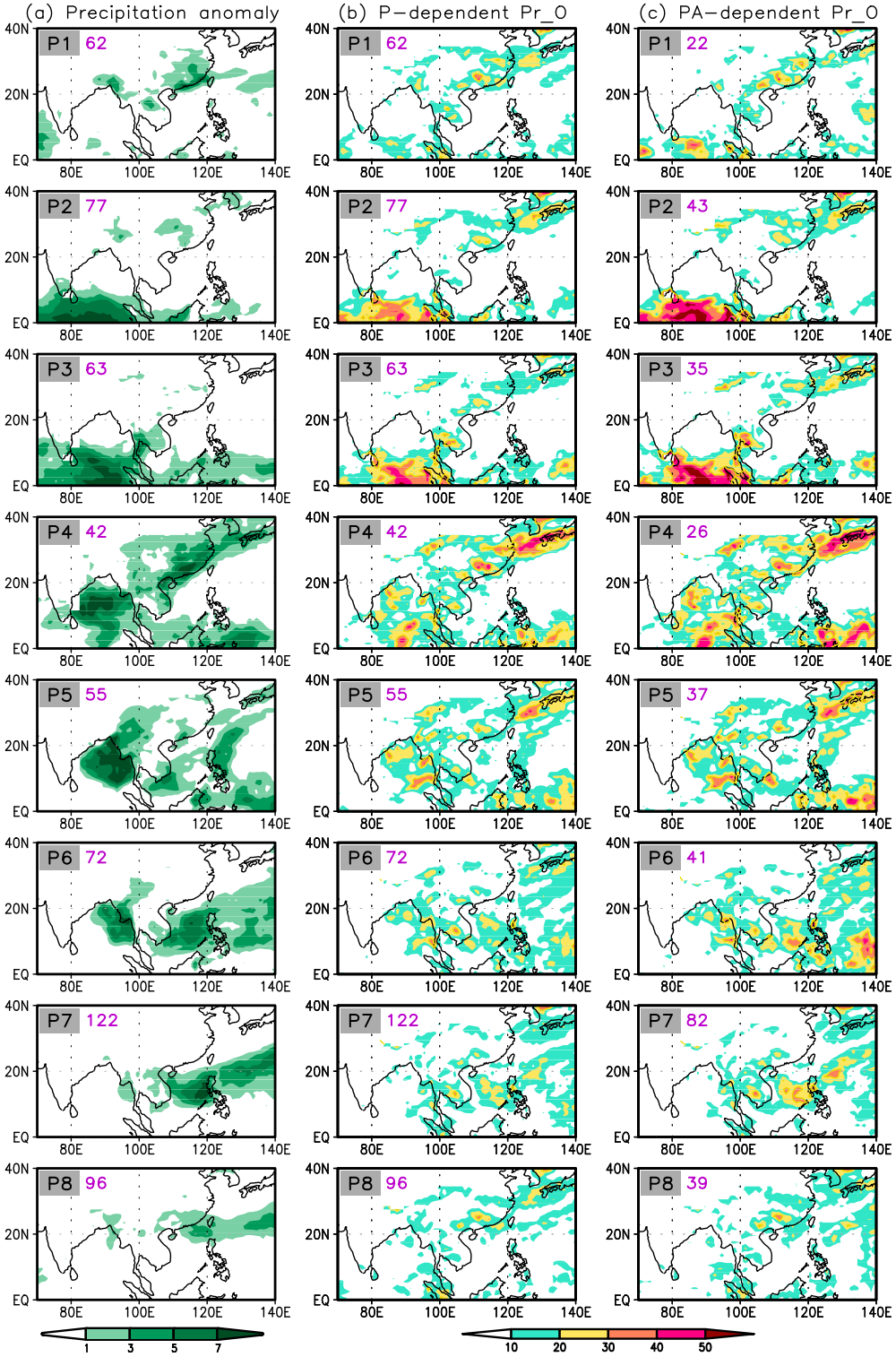

FIG. 3. (a) Precipitation anomaly (mm day^{-1}), (b) P-dependent probability (%), and (c) PA-dependent probability (%) of extreme precipitation at each phase of BSISO1 in May. The numbers at the top-left corners in (a) and (b) indicate the total occurrence days of each BSISO1 phase. The numbers at the top-left corners in (c) is the total occurrence days of each BSISO1 phase with large amplitude.

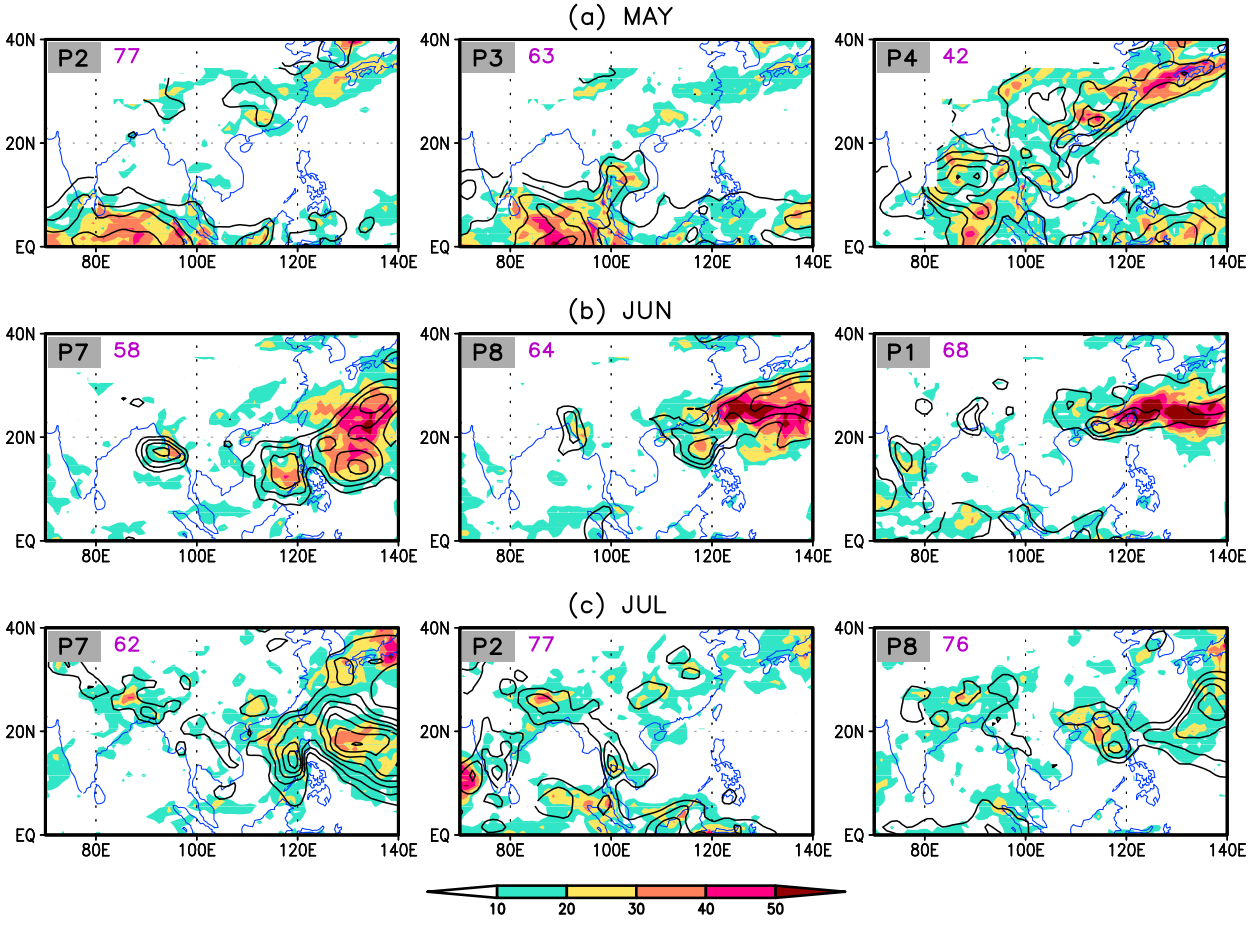

FIG. 4. P-dependent probability (%; shading) and precipitation anomaly (mm day^{-1}; contour interval is 2 mm day^{-1}, starting at 1 mm day^{-1}) during three key phases of BSISO1 in (a) May, (b) June, and (c) July. Three key phases are selected by PCC between the BSISO precipitation anomaly and P-dependent probability of extreme precipitation events (0°–40°N, 70°–140°E). The numbers at the top-left corners of each panel indicates the total occurrence days of each BSISO1 phase.

fields. Figure 6 shows the top two BSISO2 phases in each month. Precipitation anomalies at these phases also contribute to the occurrence of extreme precipitation events to some extent. The P-dependent probability is very high (about 40%–50%) over the equatorial Indian Ocean at BSISO2 phase 2 in May, the East China Sea at phase 4 in June, and the South China Sea at phase 3 in August.

What is an advantage of utilizing BSISO information as an indicator of extreme precipitation events? To address this question, the climatological probability of extreme precipitation events that are not related to BSISO activity is compared with the BSISO-based probability. Figure 7 presents the climatological and PA-dependent probabilities of extreme precipitation events over Indochina and southeastern China. These regions are important for the global rice market (e.g., Chen and Yoon 2000) and are vulnerable to flooding (Jonkman 2005; Mirza 2011). The overall climatological probability over these regions is about 10%–15% in May. During BSISO1 phase 4, the PA-dependent probability increases up to 30%–40% over southeastern China. The PA-dependent probability is quite low (less than 10%) over Indochina during BSISO1 phase 2. In August, compared to the climatological probability, the PA-dependent probability during phases 5 and 7 is very high over the Bay of Bengal, Indochina, and west of the Philippines. This indicates that we can specify the timing and area of high probability based on the BSISO information including phase and amplitude. These results demonstrate an obvious advantage of using BSISO to predict extreme precipitation events.

5. Possibility of predicting extreme precipitation events using BSISO forecasts

In the previous section, it is suggested that the BSISO indices can be a useful indicator for forecasting extreme

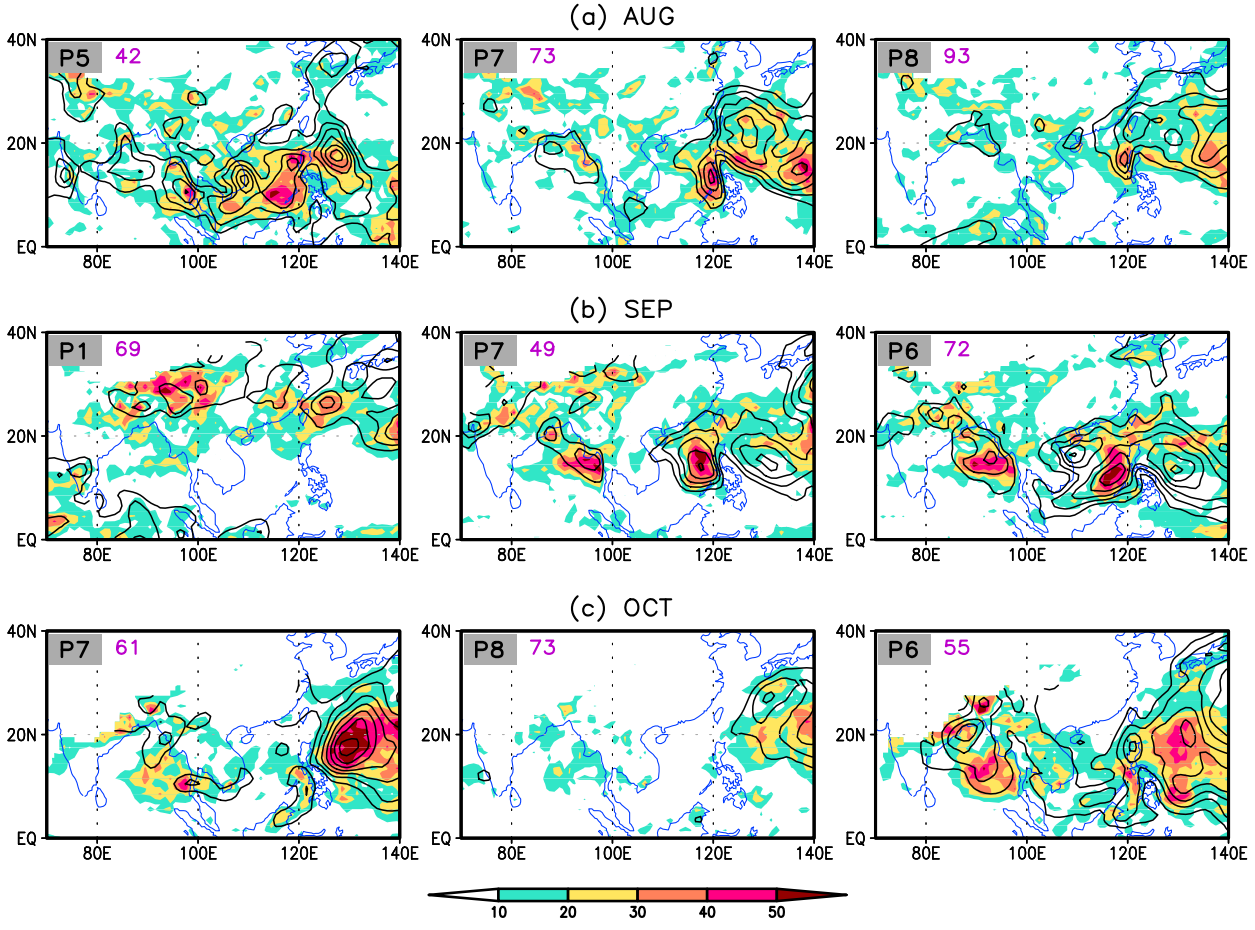

FIG. 5. As in Fig. 4, but for (a) August, (b) September, and (c) October.

precipitation events. To evaluate our finding we estimate the probability of extreme events using predicted BSISO indices and compare it with observed results. Although three years of BSISO forecast data from APCC may not be sufficient to estimate probability of extreme precipitation occurrence, our results would be helpful to verify the usefulness of real-time BSISO forecasts for the prediction of extreme precipitation events over Asia.

Before calculating the probability of extreme events using BSISO forecasts, we evaluate the prediction skill of leading BSISO modes. The prediction skill of BSISO indices vary with model, initial season, and initial amplitude of BSISO (Lee et al. 2015; Lee and Wang 2016). In the present study, the dependence of BSISO prediction skill to initial season (i.e., the month in which prediction is initiated) is examined. Figure 8 shows the bivariate correlation skill of BSISO forecast data provided by three models of APCC. The prediction skill is determined by the forecast lead day when the correlation drops below a threshold of 0.5. The correlation skills of BSISO1 and BSISO2 vary considerably with the initial season. The ECM exhibits the best skill for both BSISO1 (>15 days) and BSISO2 (>13 days) except in May. BSISO1 tends to show high skill when initialized in September or October, whereas the skill of BSISO2 tends be high when initialized in June or July. Interestingly, all three models show the lowest skills for BSISO1 and BSISO2 when initialized in May. Because BSISO prediction skill is higher than 1 week in most cases, we can expect the pentad 2 and pentad 3 forecasts to be able to capture the empirical relationship between BSISO and extreme precipitation events to some extent.

Figure 9 depicts the P-dependent probability of extreme precipitation events determined by observed BSISO and BSISO forecasts of pentad 2, respectively. For a fair comparison, the observed probability (i.e., Pr_O) in Fig. 9 is calculated using observed BSISO indices from 2013 to 2015. The probability patterns estimated by BSISO forecasts (i.e., Pr_F) exhibit similar distribution to observations although the forecast lead time of the pentad 2 forecast is relatively long (9–13 days). Major regions with high probability such as the WNP and

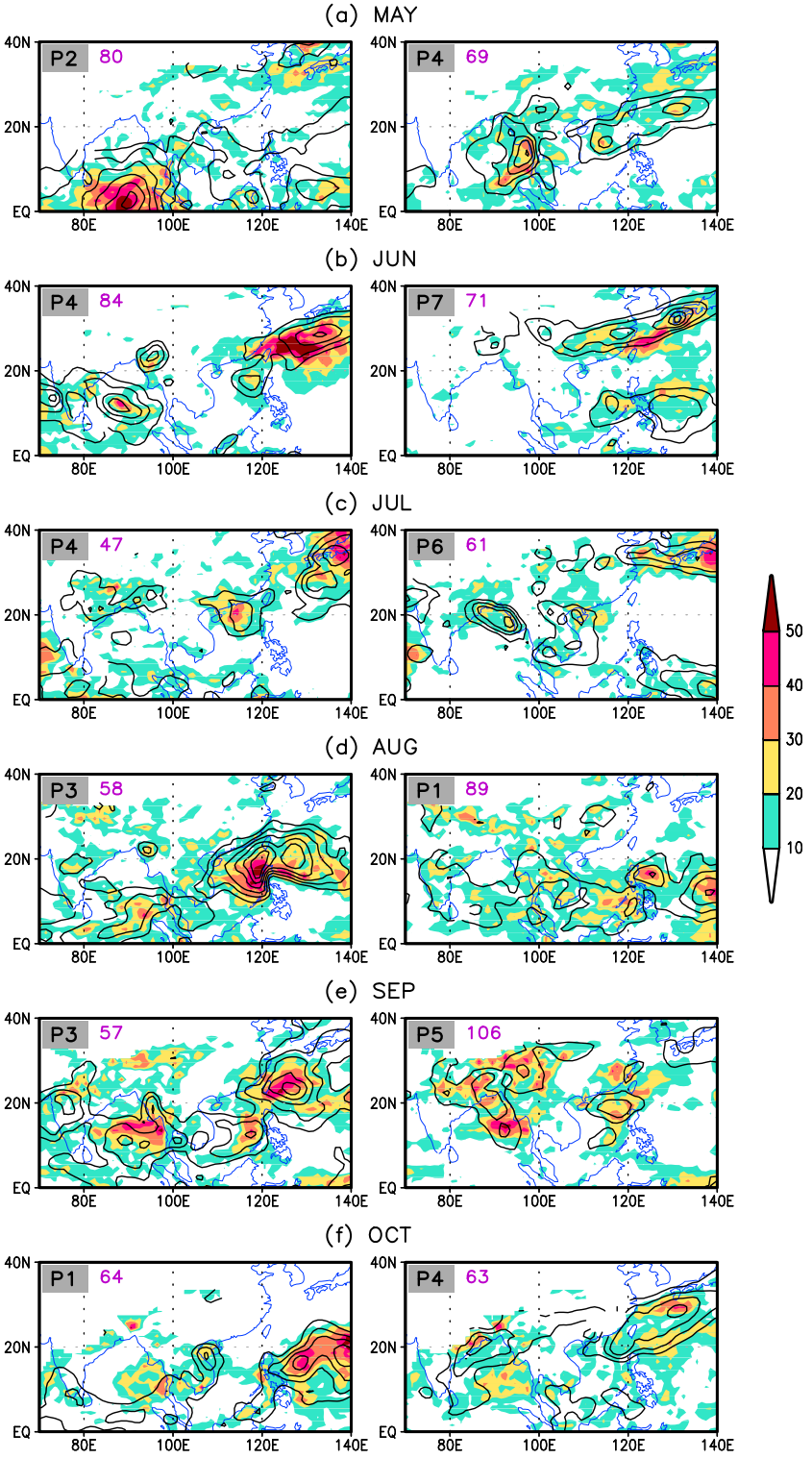

FIG. 6. P-dependent probability (%; shading) and precipitation anomaly (mm day^{-1}; contour interval is 2 mm day^{-1}, starting at 1 mm day^{-1}) during key phases of BSISO2 in (a) May, (b) June, (c) July, (d) August, (e) September, and (f) October. Two key phases are selected by PCC between the BSISO precipitation anomaly and P-dependent probability of extreme precipitation events (0°–40°N, 70°–140°E). The numbers at top-left corners in each panel indicates the total occurrence days of each BSISO2 phase.

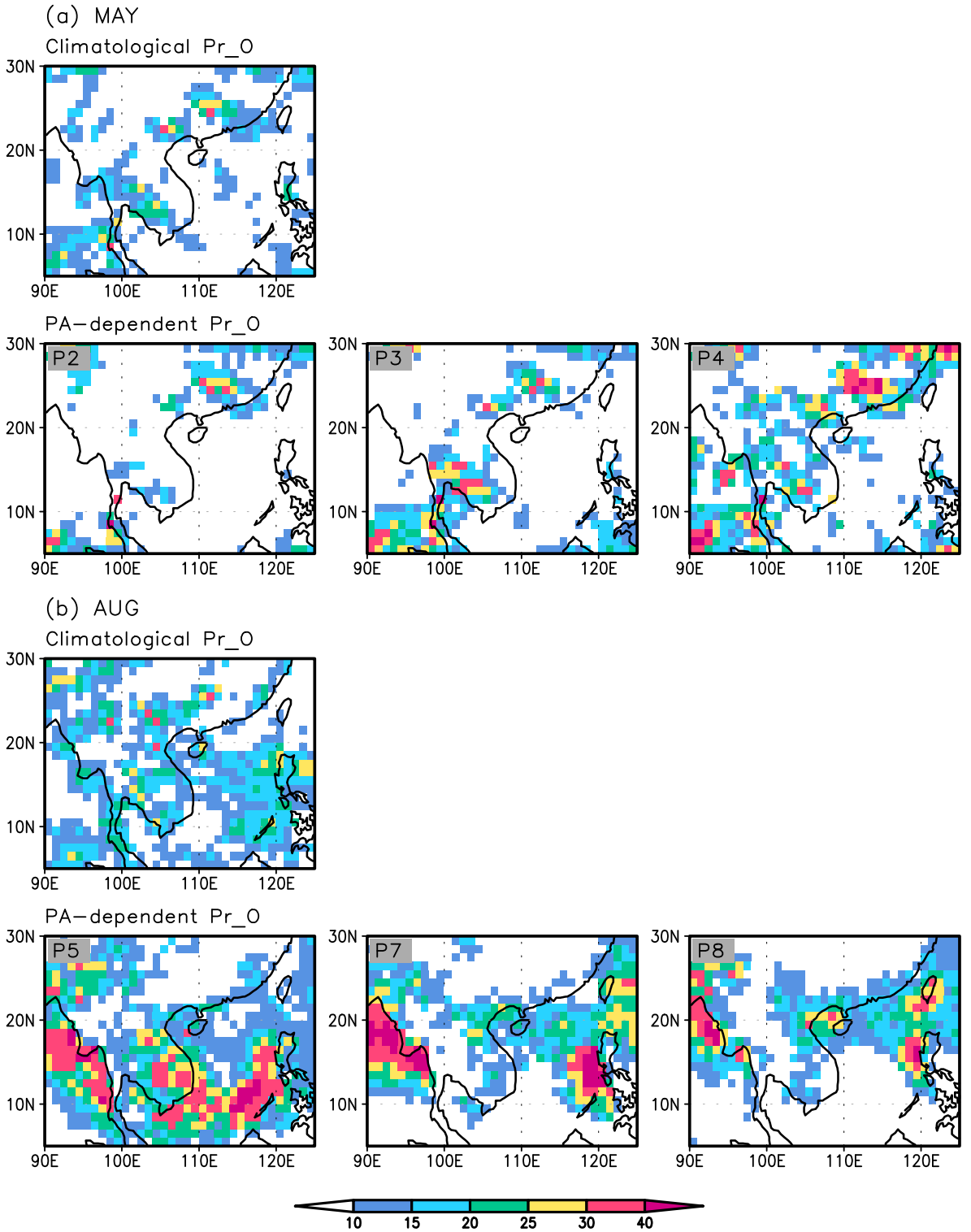

FIG. 7. Climatological and PA-dependent probabilities of extreme precipitation events in (a) May and (b) August. The PA-dependent probability of extreme precipitation is estimated by each phase of BSISO1 with large amplitude.

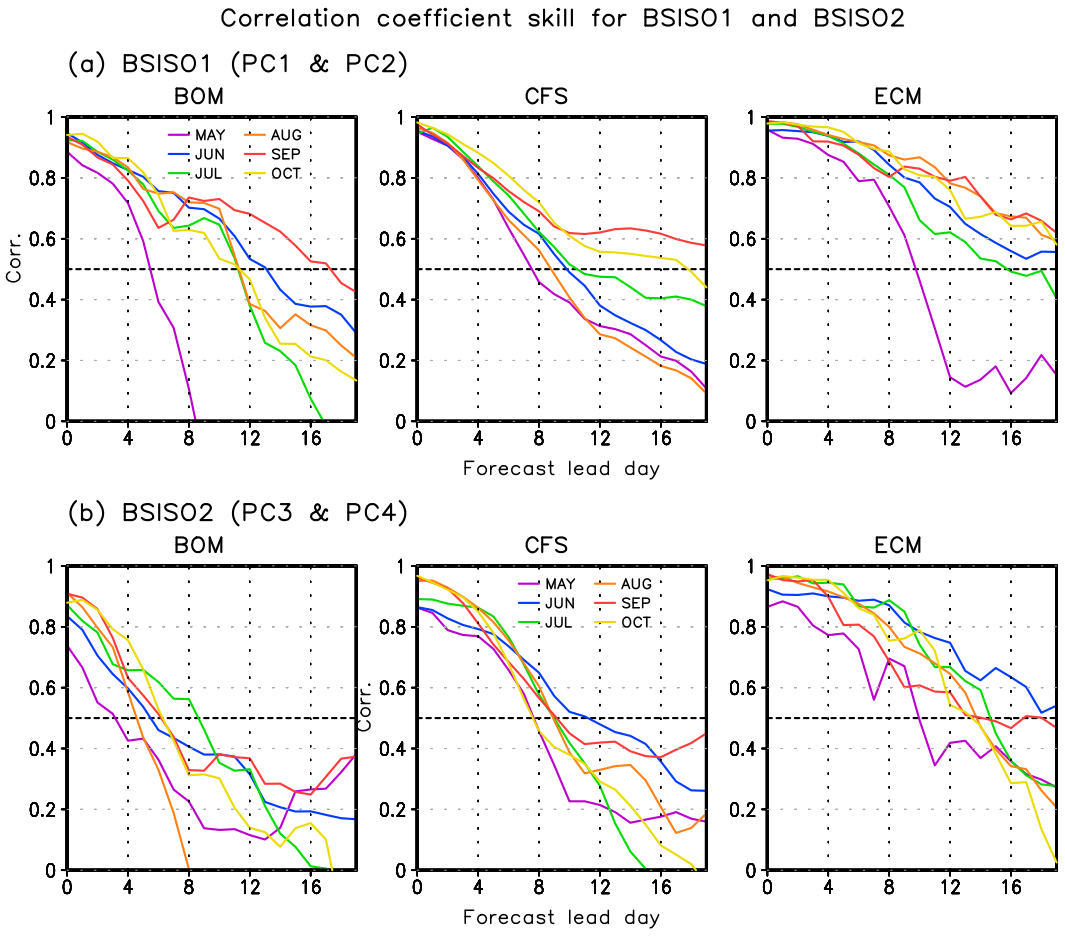

FIG. 8. Bivariate correlation coefficients for (a) BSISO1 (PC1 and PC2) and (b) BSISO2 (PC3 and PC4).

South China Sea during BSISO1 phase 7 in July are captured in all models.

Furthermore, to evaluate the capability of real-time BSISO forecasts for predicting extreme events quantitatively, we examine the PCC skill score between the probability distributions estimated by observed and predicted BSISO indices (i.e., PCC between Pr_O and Pr_F). The PCC is calculated over the region 0°–40°N, 70°–140°E, but only for the grid points where the probability derived from observed BSISO is greater than 5%.

Figure 10 presents the PCC skill score for P-dependent probability of extreme precipitation estimated by BSISO1 of the pentad 3 forecast (14–18 forecast lead days). The BSISO1 phase that occurs less than 5 days over three years (2013–15) is excluded in this analysis. Since ECM shows superior prediction capability of the leading BSISO modes as shown in Fig. 8, the PCC skill score of the ECM forecast is high in most cases. In some cases such as phase 5 in September and phase 7 in October, the PCC skill score is very high, exceeding 0.8. The PCC skill score is very low in May (not shown), and this may be attributed to the low skill of BSISO in May (Fig. 8). Consequently, Figs. 9 and 10 support the potential for subseasonal prediction of extreme precipitation events 1–2 weeks ahead using real-time BSISO forecasts.

6. Summary and discussion

Forecasting extreme precipitation events is one of the challenges in climate prediction. The main objectives of this study are to establish the useful relationship between BSISO activity and extreme precipitation occurrence and to apply its empirical relationship to the subseasonal prediction of extreme precipitation events. The probability of extreme precipitation is estimated based on the BSISO phase and amplitude. Additionally, we evaluate the prediction skill of BSISO forecast data provided by APCC and the capability of BSISO forecasts to capture the empirical linkage between BSISO activity and extreme precipitation events.

Our major findings are summarized as follows:

- The extreme precipitation probability changes from less than 10% to over 40%–50% according to BSISO phases at a given area and month (Fig. 3). The probability

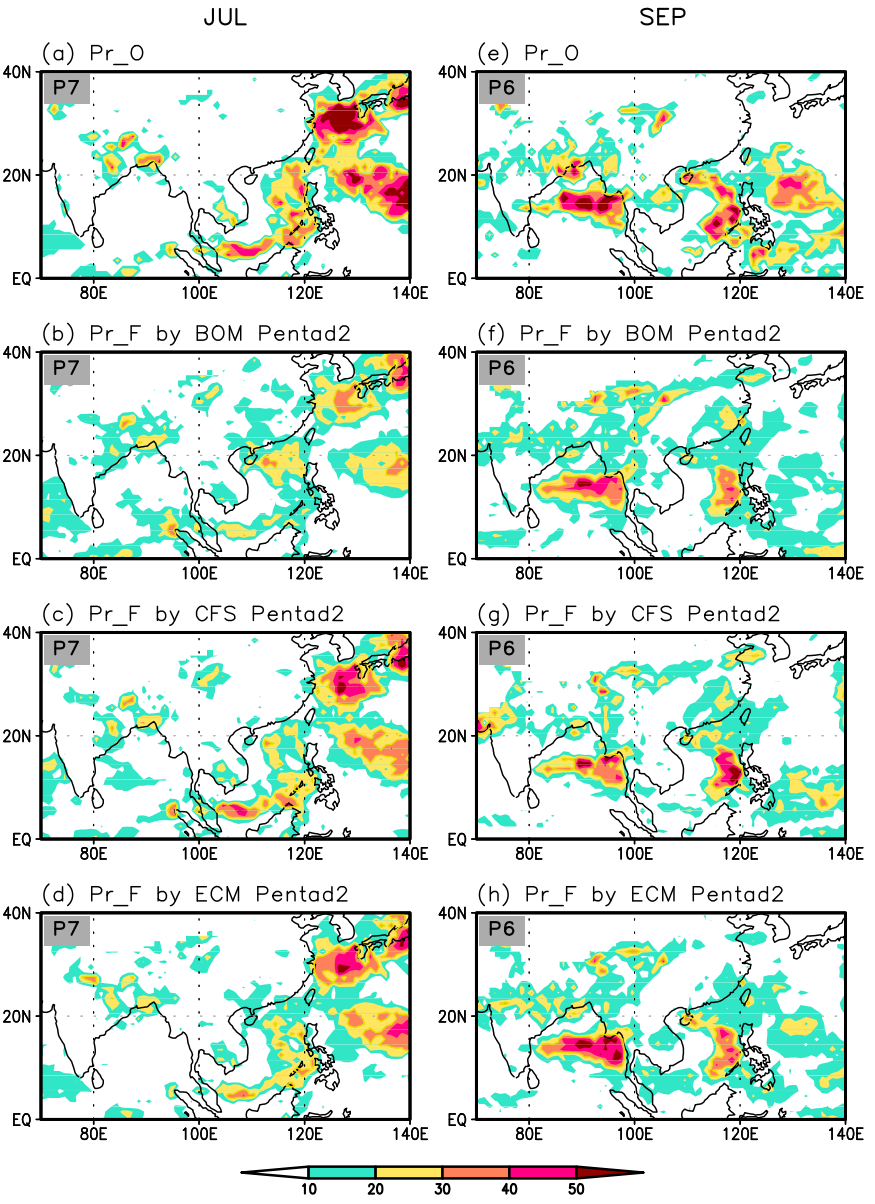

FIG. 9. The P-dependent probability of extreme precipitation estimated by (a),(e) the observed BSISO1 and (b)–(d) and (f)–(h) the BSISO1 forecast of pentad 2, for (left) BSISO1 phase 7 in July and (right) phase 6 in September.

of extreme precipitation events tends to be high when BSISO amplitude is large. Therefore, use of BSISO information including phase and amplitude facilitates identifying area and timing of high probability of extreme precipitation occurrence (Fig. 7).

- In general, the probability of extreme precipitation estimated by BSISO activity is high over ocean. Particularly, it is greater than 40% over the Indian Ocean in May, the East China Sea in June, and the WNP in October when BSISO precipitation anomaly is strong over the corresponding regions.
- Occurrence of extreme precipitation over some land regions is highly controlled by BSISO activity (Figs. 4 and 5). Probability of extreme precipitation over southeastern China is 30%–40% in May when the BSISO precipitation anomaly arrives over the region (BSISO1 phase 4). Similarly, the extreme precipitation probability over western China reaches about 40%–50% in September when the BSISO precipitation anomaly occurs over the corresponding region (BSISO1 phase 1).
- BSISO forecasts at lead times longer than two weeks can capture the empirical relationship between BSISO

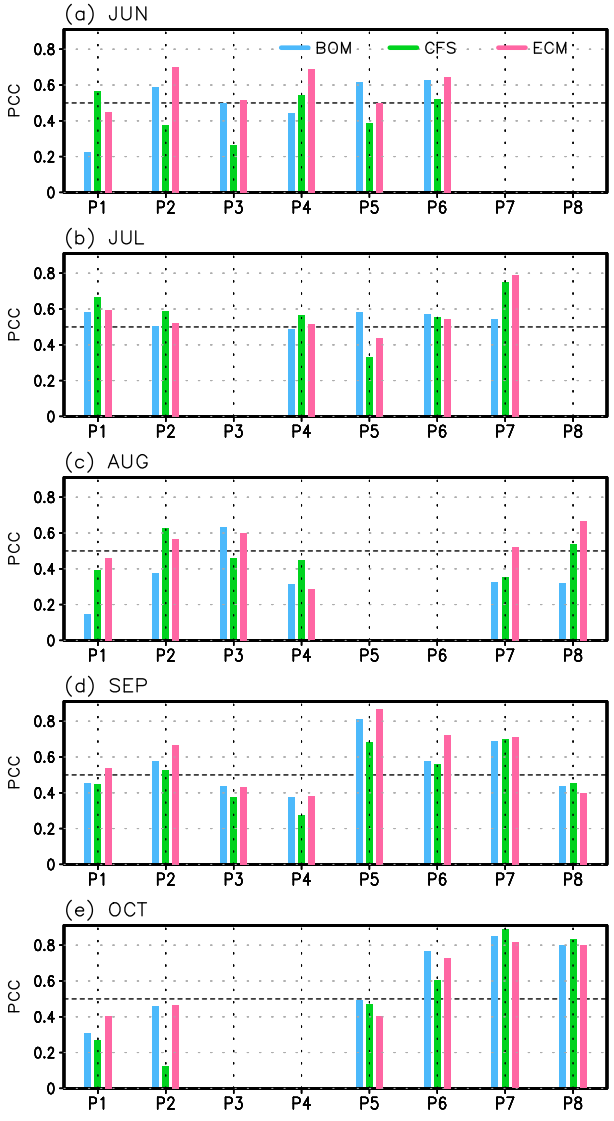

FIG. 10. The PCC skill score for the P-dependent probability of extreme precipitation events estimated by BSISO1 of the pentad 3 forecast. The PCC is calculated in the region 0°–40°N, 70°–140°E, but using only grid points where the probability estimated by observed BSISO1 is greater than 5%.

activity and extreme precipitation events to some extent (Figs. 9 and 10). This is attributed to the useful prediction skill of real-time BSISO produced by APCC models (Fig. 8), particularly in ECM, which shows about 20 days of prediction skills except in May.

The methodology adopted in this study serves as a guideline to utilize the real-time BSISO forecasts. Our results show that the ability of real-time BSISO forecasts to capture extreme precipitation occurrence is promising. However, we need to be cautious because the three years of forecast duration are limited and not long enough to estimate the probability of extreme events from a climatological perspective. For a more thorough assessment of BSISO forecast skill and its ability of monitoring extreme precipitation occurrence, the extended forecast record (e.g., from the Subseasonal-to-Seasonal Prediction Project database; http://apps.ecmwf.int/datasets/data/s2s/levtype=sfc/type=cf/) will be required in the future work. In addition, a suitable approach to combine probabilities estimated by BSISO1 and BSISO2 needs to be developed for improvement of extreme precipitation prediction. We believe that this work encourages further investigation into a better forecast approach to predict and manage extreme precipitation events.

Our results indicate that improving the BSISO forecast can lead to better prediction and management of extreme precipitation events. In all models, prediction skills of BSISO1 and BSISO2 are the lowest in May (Fig. 8). The low prediction skill of BSISO in May is partly attributed to small BSISO amplitude in the corresponding month (Lee et al. 2013) because the BSISO prediction skill with large initial amplitude is better than that with small initial amplitude (Lee et al. 2015). Another possible reason is a model's capability to capture the annual cycle of SST and low-level moisture distribution since the character of the ISO tends to depend on these factors (Wang and Xie 1997; Kemball-Cook and Wang 2001). In early summer, the northeastern Indian Ocean, Bay of Bengal, and Arabian Sea are warmer than 29°C and their ability to support deep convection and low-level moisture is substantially greater over these regions compared with other months (Kemball-Cook and Wang 2001). The model's deficiency in capturing these aspects may be responsible for the poor simulation of the ISO in early summer. This shortcoming can be improved by a realistic atmospheric initialization to some extent. Alessandri et al. (2015) showed that the realistic phase initialization of ISO modes improves the forecast skill of Indian summer monsoon onset triggered by northward propagating ISO mode.

Meanwhile, a noticeable phase preference of BSISO activity is found (Fig. 2). BSISO1 phase 7 in May, phase 2 in August, phase 5 in September, and phase 1 in October are the most frequently occurring phases at a given month. We speculate that these phases are likely associated with the persistence of the corresponding phase. Figure 11 depicts the duration days of BSISO1 phase in each month. Here the duration days of each phase indicate the consecutive days of a certain phase after its occurrence. It is noted that the most frequently occurring phases tend to persist for many days once they appear. Since social and economic impacts of extreme precipitation depend on the duration of extreme precipitation events, more work on the BSISO behavior including the physical mechanism of

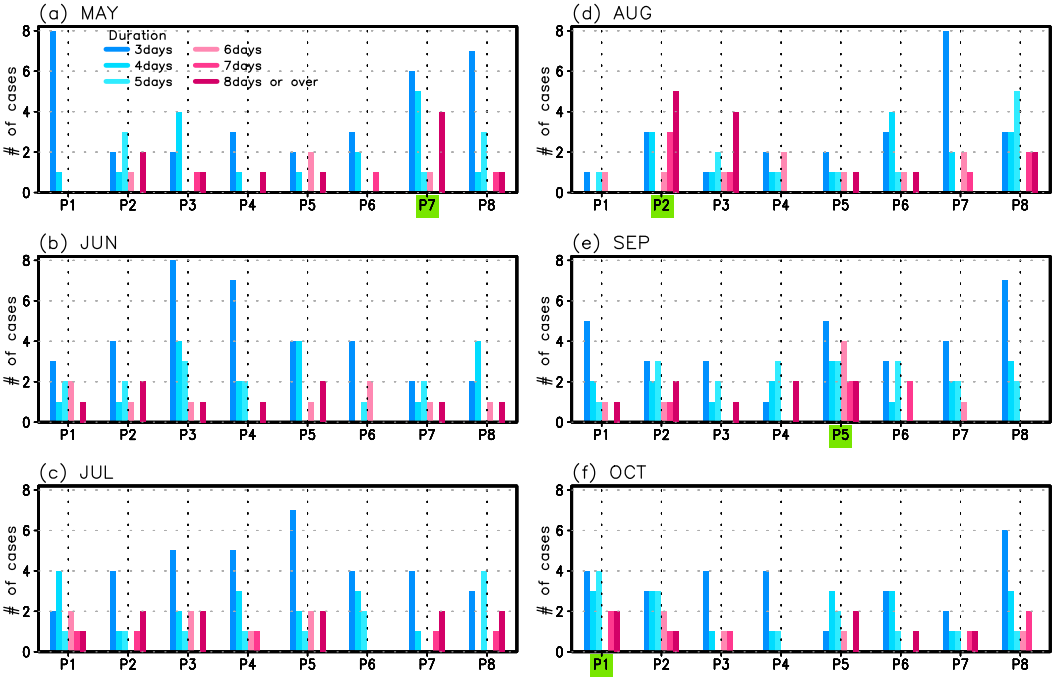

FIG. 11. Number of cases categorized by duration days of each BSISO1 phase. The duration days indicate the consecutive days of a certain phase after it occurs. The most frequently occurring BSISO1 phases as shown in Fig. 2 are highlighted in green.

long-lasting phase, transition between phases, and phase-locking of ISO to annual cycle (Wang and Xu 1997) will be of great value for improving prediction capability of extreme precipitation events.

Acknowledgments. This work was jointly supported by APEC Climate Center (APCC) and the National Research Foundation (NRF) of Korea through a Global Research Laboratory (GRL) grant of the Korean Ministry of Education, Science and Technology (MEST; Grant 2011-0021927).

REFERENCES

Adhikari, P., Y. Hong, K. R. Douglas, D. B. Kirschbaum, J. Gourley, R. Adler, and G. R. Brakenridge, 2010: A digitized global flood inventory (1998–2008): Compilation and preliminary results. *Nat. Hazards*, **55**, 405–422, doi:10.1007/s11069-010-9537-2.

Alessandri, A., A. Borrelli, A. Cherchi, S. Materia, A. Navarra, J.-Y. Lee, and B. Wang, 2015: Prediction of Indian summer monsoon onset using dynamical subseasonal forecasts: Effects of realistic initialization of the atmosphere. *Mon. Wea. Rev.*, **143**, 778–793, doi:10.1175/MWR-D-14-00187.1.

Buizza, R., P. L. Houtekamer, Z. Toth, G. Pellerin, M. Wei, and Y. Zhu, 2005: A comparison of the ECMWF, MSC, and NCEP global ensemble prediction systems. *Mon. Wea. Rev.*, **133**, 1076–1097, doi:10.1175/MWR2905.1.

Chen, T.-C., and J.-H. Yoon, 2000: Interannual variation in Indochina summer monsoon rainfall: Possible mechanism. *J. Climate*, **13**, 1979–1986, doi:10.1175/1520-0442(2000)013<1979:IVIISM>2.0.CO;2.

Dewan, T. H., 2015: Societal impacts and vulnerability to floods in Bangladesh and Nepal. *Wea. Climate Extremes*, **7**, 36–42, doi:10.1016/j.wace.2014.11.001.

Ding, Q., and B. Wang, 2009: Predicting extreme phases of the Indian summer monsoon. *J. Climate*, **22**, 346–363, doi:10.1175/2008JCLI2449.1.

Endo, N., J. Matsumoto, and T. Lwin, 2009: Trends in precipitation extremes over Southeast Asia. *Sci. Online Lett. Atmos.*, **5**, 168–171, doi:10.2151/sola.2009-043

Goswami, B. N., 2011: South Asian monsoon. *Intraseasonal Variability of the Atmosphere–Ocean Climate System*, 2nd ed. W. K.-M. Lau and D. E. Waliser, Eds., Springer, 21–72.

——, R. S. Ajayamohan, P. K. Xavier, and D. Sengupta, 2003: Clustering of synoptic activity by Indian summer monsoon intraseasonal oscillations. *Geophys. Res. Lett.*, **30**, 1431, doi:10.1029/2002GL016734.

——, V. Venugopal, D. Sengupta, M. S. Madhusoodanan, and P. K. Xavier, 2006: Increasing trend of extreme rain events over India in a warming environment. *Science*, **314**, 1442–1445, doi:10.1126/science.1132027.

Gottschalck, J., and Coauthors, 2010: A framework for assessing operational Madden–Julian oscillation forecasts: A CLIVAR MJO working group project. *Bull. Amer. Meteor. Soc.*, **91**, 1247–1258, doi:10.1175/2010BAMS2816.1.

Hsu, P.-C., J.-Y. Lee, and K.-J. Ha, 2016: Influence of boreal summer intraseasonal oscillation on rainfall extremes in southeast China. *Int. J. Climatol.*, **36**, 1403–1412, doi:10.1002/joc.4433.

Hudson, D., A. G. Marshall, Y. Yin, O. Alves, and H. H. Hendon, 2013: Improving intraseasonal prediction with a new ensemble generation strategy. *Mon. Wea. Rev.*, **141**, 4429–4449, doi:10.1175/MWR-D-13-00059.1.

Huffman, G. J., and D. T. Bolvin, 2013: Version 1.2 GPCP one-degree daily precipitation data set documentation. Goddard Space Flight Center, 27 pp. [Available online at ftp://precip.gsfc.nasa.gov/pub/1dd-v1.2/1DD_v1.2_doc.pdf.]

Jones, C., and L. M. V. Carvalho, 2012: Spatial–intensity variations in extreme precipitation in the contiguous United States and the Madden–Julian oscillation. *J. Climate*, **25**, 4989–4913, doi:10.1175/JCLI-D-11-00278.1.

——, D. E. Waliser, K. M. Lau, and W. Stern, 2004: Global occurrences of extreme precipitation events and the Madden–Julian oscillation: Observations and predictability. *J. Climate*, **17**, 4575–4589, doi:10.1175/3238.1.

Jonkman, S. N., 2005: Global perspectives on loss of human life caused by floods. *Nat. Hazards*, **34**, 151–175, doi:10.1007/s11069-004-8891-3.

Kemball-Cook, S., and B. Wang, 2001: Equatorial waves and air–sea interaction in the boreal summer intraseasonal oscillation. *J. Climate*, **14**, 2923–2942, doi:10.1175/1520-0442(2001)014<2923:EWAASI>2.0.CO;2.

Krishnamurthy, C. K. B., U. Lall, and H.-H. Kwon, 2009: Changing frequency and intensity of rainfall extremes over India from 1951 to 2003. *J. Climate*, **22**, 4737–4746, doi:10.1175/2009JCLI2896.1.

Kundzewicz, Z., and Coauthors, 2014: Flood risk and climate change: Global and regional perspectives. *Hydrol. Sci. J.*, **59**, 1–28, doi:10.1080/02626667.2013.857411.

Lee, J.-Y., B. Wang, M. Wheeler, X. Fu, D. Waliser, and I.-S. Kang, 2013: Real-time multivariate indices for the boreal summer intraseasonal oscillation over the Asian summer monsoon region. *Climate Dyn.*, **40**, 493–509, doi:10.1007/s00382-012-1544-4.

Lee, S.-S., and B. Wang, 2016: Regional boreal summer intraseasonal oscillation over Indian Ocean and western Pacific: Comparison and predictability study. *Climate Dyn.*, **46**, 2213–2229, doi:10.1007/s00382-015-2698-7.

——, ——, D. E. Waliser, J. M. Neena, and J.-Y. Lee, 2015: Predictability and prediction skill of the boreal summer intraseasonal oscillation in the Intraseasonal Variability Hindcast Experiment. *Climate Dyn.*, **45**, 2123–2135, doi:10.1007/s00382-014-2461-5.

Liebmann, B., H. Hendon, and J. Glick, 1994: The relationship between tropical cyclones of the western Pacific and Indian Oceans and the Madden–Julian oscillation. *J. Meteor. Soc. Japan*, **72**, 401–412.

Lin, H., G. Brunet, and J. Derome, 2008: Forecast skill of the Madden–Julian oscillation in two Canadian atmospheric models. *Mon. Wea. Rev.*, **136**, 4130–4149, doi:10.1175/2008MWR2459.1.

Liu, F., and B. Wang, 2014: A mechanism for explaining the maximum intraseasonal oscillation center over the western North Pacific. *J. Climate*, **27**, 958–968, doi:10.1175/JCLI-D-12-00797.1.

Maloney, E., and D. Hartmann, 2001: The Madden–Julian oscillation, barotropic dynamics, and North Pacific tropical cyclone formation. Part I: Observations. *J. Atmos. Sci.*, **58**, 2545–2558, doi:10.1175/1520-0469(2001)058<2545:TMJOBD>2.0.CO;2.

Mirza, M. M. Q., 2011: Climate change, flooding in South Asia and implications. *Reg. Environ. Change*, **11** (Suppl. 1), 95–107, doi:10.1007/s10113-010-0184-7.

Moon, J.-Y., B. Wang, and K.-J. Ha, 2012: MJO modulation on 2009/10 winter snowstorms in the United States. *J. Climate*, **25**, 978–991, doi:10.1175/JCLI-D-11-00033.1.

——, ——, ——, and J.-Y. Lee, 2013: Teleconnections associated with Northern Hemisphere summer monsoon intraseasonal oscillation. *Climate Dyn.*, **40**, 2761–2774, doi:10.1007/s00382-012-1394-0.

Saha, S., and Coauthors, 2014: The NCEP Climate Forecast System version 2. *J. Climate*, **27**, 2185–2208, doi:10.1175/JCLI-D-12-00823.1.

Sen Roy, S., and R. C. Balling Jr., 2004: Trends in extreme daily precipitation indices in India. *Int. J. Climatol.*, **24**, 457–466, doi:10.1002/joc.995.

Vitart, F., W. Robertson, and D. L. T. Anderson, 2012: Subseasonal to Seasonal Prediction Project: Bridging the gap between weather and climate. *WMO Bull.*, **61**, 23–28.

Waliser, D. E., 2006: Intraseasonal variability. *The Asian Monsoon*, B. Wang, Ed., Springer, 203–257.

Wang, B., 1992: The vertical structure and development of the ENSO anomaly mode during 1979–1989. *J. Atmos. Sci.*, **49**, 698–712, doi:10.1175/1520-0469(1992)049<0698:TVSADO>2.0.CO;2.

——, and X. Xie, 1997: A model for the boreal summer intraseasonal oscillation. *J. Atmos. Sci.*, **54**, 72–86, doi:10.1175/1520-0469(1997)054<0072:AMFTBS>2.0.CO;2.

——, and X. Xu, 1997: Northern Hemisphere summer monsoon singularities and climatological intraseasonal oscillation. *J. Climate*, **10**, 1071–1085, doi:10.1175/1520-0442(1997)010<1071:NHSMSA>2.0.CO;2.

——, and J.-Y. Moon, 2017: Sub-seasonal prediction of extreme weather events. *Bridging Science and Policy Implication for Managing Climate Extremes: Linking Science and Policy Implications*, C.-S. Chung and B. Wang, Eds., World Scientific Series of Asia-Pacific Weather and Climate Press, in press.

——, Q. Ding, and J.-G. Jhun, 2006: Trends in Seoul (1778–2004) summer precipitation. *Geophys. Res. Lett.*, **33**, L15803, doi:10.1029/2006GL026418.

Wu, R., and B. Wang, 2000: Interannual variability of summer monsoon onset over the western North Pacific and the underlying processes. *J. Climate*, **13**, 2483–2501, doi:10.1175/1520-0442(2000)013<2483:IVOSMO>2.0.CO;2.

Xavier, P., R. Rahmat, W. K. Cheong, and E. Wallace, 2014: Influence of Madden–Julian oscillation on Southeast Asia rainfall extremes: Observations and predictability. *Geophys. Res. Lett.*, **41**, 4406–4412, doi:10.1002/2014GL060241.

Yao, C., W. Qian, S. Yang, and Z. Lin, 2010: Regional features of precipitation over Asia and summer extreme precipitation over Southeast Asia and their associations with atmospheric–oceanic conditions. *Meteor. Atmos. Phys.*, **106**, 57–73, doi:10.1007/s00703-009-0052-5.

Zhai, P., X. Zhang, H. Wan, and X. Pan, 2005: Trends in total precipitation and frequency of daily precipitation extremes over China. *J. Climate*, **18**, 1096–1108, doi:10.1175/JCLI-3318.1.

Zhang, C., 2013: Madden–Julian oscillation: Bridging weather and climate. *Bull. Amer. Meteor. Soc.*, **94**, 1849–1870, doi:10.1175/BAMS-D-12-00026.1.

Zhou, S., M. L'Heureux, S. Weaver, and A. Kumar, 2012: A composite study of the MJO influence on the surface air temperature and precipitation over the continental United States. *Climate Dyn.*, **38**, 1459–1471, doi:10.1007/s00382-011-1001-9.

Zhu, C., T. Nakazawa, J. Li, and L. Chen, 2003: The 30–60 day intraseasonal oscillation over the western North Pacific Ocean and its impacts on summer flooding in China during 1998. *Geophys. Res. Lett.*, **30**, 1952, doi:10.1029/2003GL017817.